FRACAS: A capacity spectrum approach for seismic fragility assessment including record-to-record variability

Tiziana Rossetto [a,*], Pierre Gehl [a,b], Stylianos Minas [a], Carmine Galasso [a], Philippe Duffour [a], John Douglas [c], Oliver Cook [a]

[a] EPICentre, Department of Civil, Environmental & Geomatic Engineering, University College London, Gower Street, WC1E 6BT London, UK
[b] Risks and Prevention Division, BRGM, 3 Avenue Claude Guillemin, 45060 Orléans, France
[c] Department of Civil and Environmental Engineering, University of Strathclyde, James Weir Building, 75 Montrose Street, Glasgow G1 1XJ, UK

ARTICLE INFO

ABSTRACT

This paper presents a new approach for the derivation of fragility curves, named FRAgility through Capacity spectrum ASsessment (FRACAS). FRACAS adapts the capacity spectrum assessment method and uses inelastic response spectra derived from earthquake ground motion accelerograms to construct fragility curves. Following a description of the FRACAS approach, the paper compares the predicted maximum interstory drift (MIDR) response obtained from FRACAS and nonlinear time history analyses (NLTHA) for two case-study buildings subjected to 150 natural accelerograms. FRACAS is seen to represent well the response of both case-study structures when compared to NLTHA. Observations are made as to the sensitivity of the derived fragility curves to assumptions in the capacity spectrum assessment and fragility curve statistical model fitting. The paper also demonstrates the ability of FRACAS to capture inelastic record-to-record variability and to properly translate this into the resulting fragility curves.

© 2016 The Authors. Published by Elsevier Ltd. This is an open access article under the CC BY license (http://creativecommons.org/licenses/by/4.0/).

1. Introduction

Fragility curves are a key component of probabilistic seismic risk assessment. They express continuous relationships between a ground motion intensity measure (IM) and the probability that the specified structure will reach or exceed predefined damage states; they can be expressed as

$$P(DS \geqslant ds_i | IM), \tag{1}$$

where DS is the damage state of the asset class being assessed and ds_i is a particular predefined state of damage. An IM is a scalar ground motion parameter that is considered to be representative of the earthquake damage potential with respect to the specific structure. In general terms, a fragility curve is built by fitting a statistical model to data on building damage at different values of the IM, for example based on post-earthquake surveys. In the case of analytical fragility curves, structural response is first obtained through the analysis of structural models subjected to earthquake excitation of increasing intensity. The structural response obtained is expressed in terms of engineering demand parameters (EDPs), which are then compared to properly calibrated thresholds (still in terms of EDPs) associated with a given damage state or performance level of structural and nonstructural components and systems. The number of structural analyses required to construct the fragility curve may be large if both variability in the structural model/capacity (i.e., modelling uncertainty) and ground motion characteristics are included. Hence, a number of approaches for fragility curve generation have been proposed in the past that either adopt a simplified structural model (e.g., a single degree of freedom - SDoF - system), analysis approach (static or dynamic), assessment method or combination of these. These have been extensively reviewed in [1].

In practice, for low- to mid-rise buildings, these approaches either adopt simplified structural models and assess their performance using full nonlinear time history analyses or adopt more complex structural models and assess their performance using variations of the capacity spectrum assessment method. The former approach commonly involves carrying out Incremental Dynamic Analysis (IDA, [2]) or its variants (e.g., [3]) on SDoF systems. More complex structural models can be utilized in IDA but the computational effort required to generate a fragility function representative of a building class (rather than a single building) using multiple earthquake records and structural models

commonly precludes their use. One of the advantages of IDA is that the effect of record-to-record variability can be explicitly included in the assessment; however, the accuracy of the assessment strongly depends on how well the structure is modelled by an SDoF system or other simplified modelling assumptions (e.g., [1]).

The capacity spectrum approach, originally proposed by Freeman et al. [4], relies on the determination of a structure's performance point by comparing the equivalent capacity and demand spectra in terms of the acceleration-displacement representation (ADRS). Several capacity spectrum assessment approaches have been proposed in the past, most notably the ATC-40 approach [5], the coefficient method in FEMA-356 [6] and the N2 method [7,8]. These approaches usually require a standardized design spectrum (e.g., code-based) and the use of a corner period to identify acceleration- and displacement-sensitive segments of the demand spectrum. Therefore, these standardized earthquake spectra are commonly defined as smooth functions that do not account for the variability present in natural spectra derived using recorded ground motions signals.

In this paper, a new capacity spectrum assessment approach named FRACAS (FRAgility through CApacity Spectrum assessment) is presented. FRACAS builds on the approach originally proposed in [9] and differs from those mentioned above in that it directly uses acceleration time histories from which both elastic and inelastic spectra are computed and used to find the performance point. It is acknowledged that response spectra do not capture the entire variability in earthquake ground motions. For example, response spectra are 'blind' to the duration of shaking and, therefore, two records, one of short duration and one much longer, but with the same spectrum would be assessed by this approach as having the same influence on the structure. However, several studies have shown that the amplitudes and shape of the elastic response spectra have a key influence on the inelastic structural response, particularly at high nonlinearity levels (e.g., [10]) and when collapse is of interest (e.g., [11]). Moreover, response spectra of earthquake ground motions do show considerable variability, even for the same magnitude and distance (and other source, path and site parameters), and these differences will be reflected in the fragility curves derived using this capacity spectrum method.

The paper first describes the FRACAS approach in detail. It then presents a comparison of the results from FRACAS and nonlinear time history analyses (NLTAs) for the case study of two regular mid-rise (4-story) reinforced concrete (RC) bare frames. These structural models are selected as they provide representative examples of both existing and modern code-conforming European RC buildings. The ability of FRACAS to effectively capture the variability of earthquake ground motions and their influence on fragility functions is then explored by employing various sets of recorded and modified ground motions accelerograms. Finally, the sensitivity of the derived fragility curves to other assumptions in the structural analysis and capacity spectrum assessment, namely, the approach followed for capacity curve idealization, and the choice of the statistical curve fitting method, are presented. This article significantly extends the preliminary analyses presented by Gehl et al. [10] and Rossetto et al. [11].

2. FRACAS: FRAgility through Capacity spectrum ASsessment

FRACAS is a procedure for fragility curve generation that builds on and improves the modified capacity spectrum method first developed by Rossetto and Elnashai [9]. FRACAS takes the basic methodology proposed in [9] and, within new software tool builds upon it to, allows more sophisticated capacity curve idealizations, the use of various hysteretic models for the SDoF in the inelastic demand calculation, and the construction of fragility functions

through several statistical model fitting techniques. The proposed approach is highly efficient and allows for fragility curves to be derived from the analysis of a specific structure or a population of frames subjected to a number of earthquake records with distinct characteristics. In this way, the method is able to account for the effect of variability in seismic input and structural characteristics on the damage statistics simulated for the building class, and evaluate the associated uncertainty in the fragility prediction.

The FRACAS procedure is based on the following steps (Fig. 1):

1. Mathematical models of a population of buildings are generated by selecting a representative building, termed "index building", and generating variations of the index building with differing structural or geometrical properties. See [1] for recommendations on how to generate the model population to represent a building class. Alternatively, large sets of structures can be generated stochastically based on statistical models of geometric and material properties (e.g., [12]).
2. The computational models of the index building and its variations are analyzed with static pushover (PO) analysis or static adaptive PO analysis (APO, e.g., [13]).
3. The PO curve is transformed into a capacity curve in ADRS space, through the use of relative floor displacements and floor masses (see Section 2.1).
4. An idealized shape is fit to the capacity curve making various choices regarding the selection of the yielding and ultimate points, the number of segments (bilinear or multilinear) and the presence of increased strength post-yield (e.g. Figs. 1a and 2).
5. The idealized curve is discretized into a number of analysis points (APs) (Fig. 1b) each representing an inelastic SDoF with the elastic stiffness, ductility and post-elastic properties shown by the capacity curve up to the considered AP.
6. At each AP, the response of the corresponding SDoF under the selected ground motion record is assessed through the Newmark-beta time-integration method. In particular, the elastic response is calculated for analysis points preceding yield and the inelastic response for those on the inelastic branch of the capacity spectrum (e.g. Fig. 1c and 1d).
7. Using both elastic and inelastic parts of the response spectrum, the performance point (PP) is estimated by the intersection of the capacity curve and response curve. No iterative process is required.
8. The selected EDP is determined from the PP by re-visiting the results of the PO analysis at the corresponding capacity curve point. Maximum interstory drift ratio (MIDR) is adopted as the EDP in FRACAS, but others can be determined if required, for example the roof-drift (RD). Different IMs associated with the given accelerogram used in the assessment are also calculated and stored.
9. Steps 6–8 are repeated for each capacity curve producing PPs (with associated IM and EDP) at different ground motion intensity levels. This can be done by either scaling up the selected accelerogram(s) to cover a range of intensities (similarly to the IDA procedure) or by using several accelerograms selected to represent different intensities of ground shaking (similarly to the *cloud* procedure; e.g., [3]). The number of PPs generated equals the product of the number of structural models, number of accelerograms and number of scaling factors used.
10. Fragility curves are constructed from the set of IM and EDP pairs through an appropriate statistical curve fitting approach (see Section 2.6).

It is important to note that, in contrast to other capacity spectrum methods, FRACAS does not rely on reduction factors or
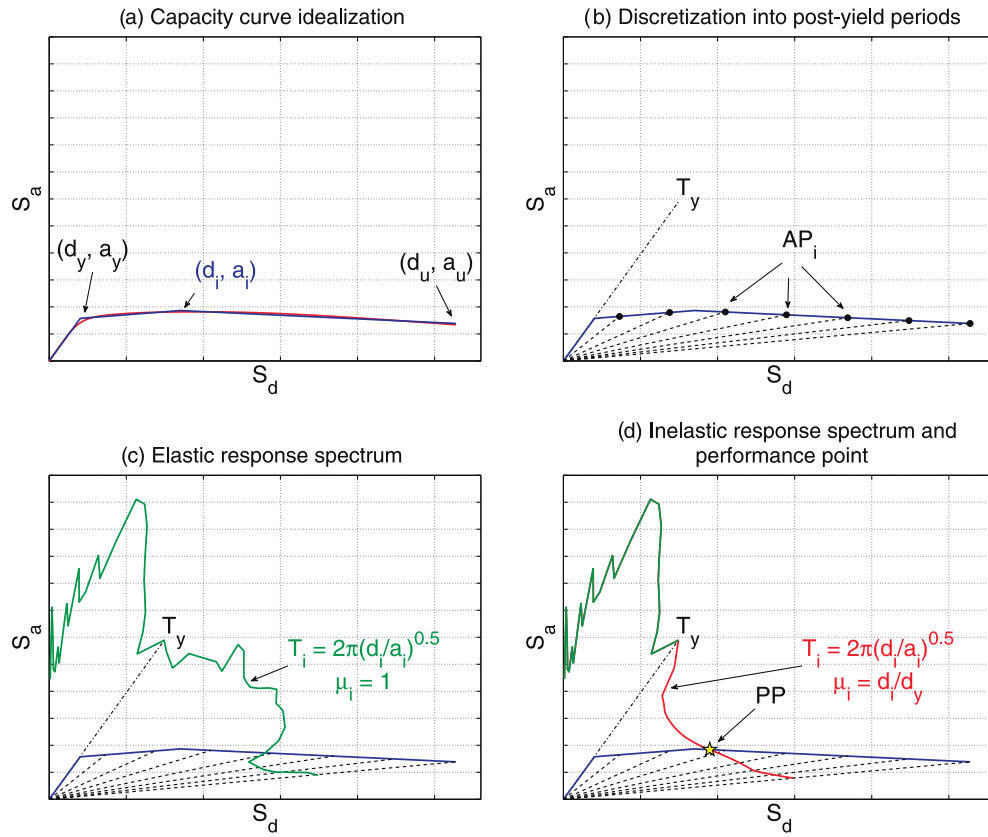
Fig. 1. Main steps of FRACAS for the derivation of the performance point (PP) using the trilinear idealization model. (a) shows the fitting of the idealised trilinear curve to the structure capacity curve; (b) shows the identification of Analysis Points (AP), (c) compares the elastic demand spectrum with the capacity curve at the point of intersection of the demand curve with the line representing the yield period of the structure; (d) shows the determination of the Performance Point (PP).
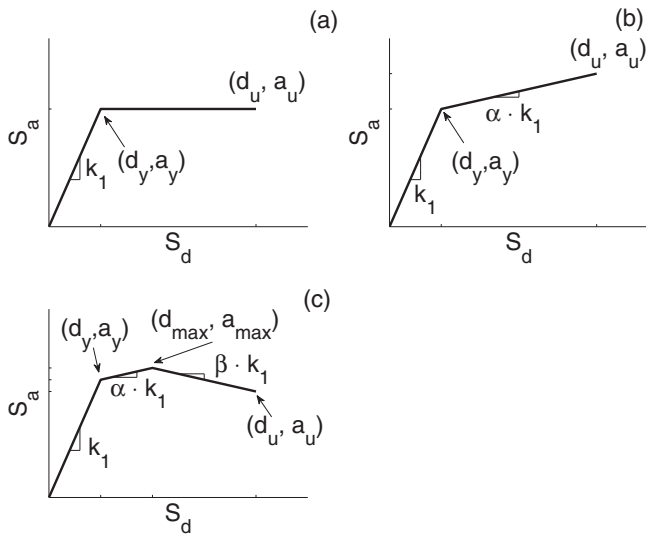

Fig. 2. Models used in FRACAS for the capacity curve idealization: (a) elastic-perfectly plastic model (EPP), (b) elastic-plastic with positive strain-hardening (EPH) and (c) tri-linear model (TL).

indices to estimate the inelastic spectrum from the elastic one. Instead, it carries out, for each AP (with target ductility and period), a simplified dynamic analysis on the idealized nonlinear SDoF model corresponding to the capacity curve. This process proves to be more time-consuming than the commonly-used static approaches but it remains faster than performing full time history analyses on finite element models of full structures. This feature also has the advantage of permitting the use of various natural, artificial or simulated accelerograms that generate unsmoothed spectra as opposed to standardized design spectra. Therefore, the record-to-record variability can be directly introduced and the resulting cloud of PPs leads to fragility curves that account for the natural variability in the seismic demand. The key steps of the FRACAS approach are explained in more detail below.

2.1. Transformation of the pushover curve to ADRS space

In the case of traditional static PO analysis the transformation of the base shear-top (i.e., roof) drift curve (PO curve) to ADRS space is done in FRACAS using the modal participation factors and effective modal weight ratios, determined from the fundamental mode of the structure, using the following equations:

$$\Gamma = \frac{\sum_{j=1}^{N} m_j \phi_j}{\sum_{j=1}^{N} m_j \phi_j^2}; \quad S_a = \frac{V_b}{M^*}; \quad S_d = \frac{u_N}{\Gamma \phi_N};$$

$$M^* = \frac{\left(\sum_{j=1}^{N} m_j \phi_j\right)^2}{\sum_{j=1}^{N} m_j \phi_j^2}. \qquad (2)$$

where N is the total number of floors, u_N is the top floor displacement, V_b is the base shear force, ϕ_j is the jth floor element of the fundamental mode shape (ϕ_I), m_j is the lumped mass at the jth floor level and M^* is the effective modal mass for the fundamental mode of vibration.

In the case of APO, the transformation must include the combined effect of multiple response modes. A single transformation cannot be applied to the APO curve as the relative contribution of each mode changes with each applied load increment. Hence,

an approximate method for the transformation is adopted, where the instantaneous displaced shape and story forces at each increment step (v) of the APO are used to transform the force displacement curves into ADRS space. The same expressions as for the SDoF transformation are adopted (Eq. (2)), with the current displaced shape of the structure normalized to the top displacement ($\underline{\phi_I}$) replacing the fundamental mode shape ($\underline{\phi_1}$). ϕ_j is then replaced with $\phi_{j,v}$, the component of $\underline{\phi_I}$ corresponding to the jth story. Also, $u_{N,v}$ and $V_{b,v}$ replace u_N and V_b, and are the top displacement and base shear at the current load increment, respectively. The reasoning behind this transformation method is that the force distribution and resulting displacement distribution implicitly incorporate the modal combinations. This assumption may not be theoretically justified, but it is observed to provide reasonable assessment results (see [14]).

2.2. Idealization of the capacity curve

In FRACAS, the capacity curve obtained from the PO is directly idealized as a multi-linear curve that: (a) is used to represent the capacity curve when it is compared to the demand values in the determination of the PPs and (b) is used to define the inelastic backbone curve of an inelastic SDoF system for the demand calculation explained in Section 2.3. Different curve shapes can currently be used to model the capacity curve of the structures: an elastic-perfectly plastic model (EPP), a non-degrading elastic-plastic with positive strain-hardening (EPH) or a tri-linear model (TL). These are illustrated in Fig. 2. The choice of model depends on the type of structure and shape of the resulting capacity curve, with, for example, EPH being better suited to steel frames without infill and TL to reinforced concrete frames with infill. Further models will be considered in the future.

Various curve fitting options are possible within FRACAS. In particular, an automated identification of the successive segments of the idealized models is provided, with three different options available for defining the yield point (d_y, a_y) (see Fig. 2):

1. First deviation from the initial stiffness (i.e. evolution of the tangent slope of the capacity curve with respect to the initial gradient – absolute deviation – or with respect to the previous gradient – relative deviation).
2. Intersection of the initial stiffness line with the maximum spectral acceleration of the capacity curve.
3. Coordinates of the nominal value of the capacity curve (i.e. secant stiffness line).

Similarly, three different options are available to define the ultimate point (d_u, a_u) (see Fig. 2):

1. The spectral displacement corresponding to the collapse drift (i.e. the last limit state in the considered damage scale).
2. The spectral displacement corresponding to the last point of the capacity curve.
3. The spectral displacement corresponding to a 20% drop of the spectral acceleration with respect to the maximum capacity.

Finally, an equal-energy criterion may also be used, where the spectral ordinate of the yield point (or the intermediate point in the case of TL) is adjusted in order to obtain the same areas under the idealized and actual capacity curves.

In addition, the manual selection of the global yield point, ultimate point and, in the case of TL, the point of the second change in slope, is also allowed. The aim in fitting the model to the capacity curve is to select the parameters of the models such that they reproduce the capacity curve as closely as possible. The different modelling options that are offered to the user are useful in emphasizing various aspects of the studied structure: one can decide whether the idealized curve must closely fit the elastic period, the maximum strength, the yield deformation or the energy dissipation capacity of the structural system. It is noted that De Luca et al. [15] have found that using the equivalent-energy criterion may lead to large biases in the prediction of the structural response, especially when the curve fitting induces a significant change in the initial stiffness.

2.3. Discretization of the idealized capacity curve and definition of a suite of SDoF systems for inelastic demand analysis

In order to improve the efficiency of the PP calculation, FRACAS discretizes the capacity curve into a number of pre- and post-yield periods, which are used as analysis points (APs). In FRACAS the number of APs is user-defined, but it is recommended that a minimum of 5 points pre-yield and 25 points post-yield (evenly distributed along the post-yield branches of the idealized curve) be used. In addition, points defining changes of slope in the idealized curve (e.g. the yield point) should always be adopted as APs. Each AP is characterized by its spectral coordinates (i.e. d_i and a_i in Fig. 1a), and a ductility value, defined by the spectral displacement of the analysis point (d_i) divided by that of the global yield of the structure (d_y). Together with the elastic period of the idealized curve, this ductility value is used to define an SDoF system from which the inelastic demand is calculated. The inelastic backbone curve of the SDoF system is also defined by the shape of the idealized curve up to the analysis point.

2.4. Inelastic demand calculation

For a given earthquake record (which could be scaled to a certain IM level), the inelastic seismic demand corresponding to each AP is calculated through the analysis of the SDoF system associated with that AP (see above). The earthquake record used in the analysis is discretized into time increments smaller than (1/50)th of the smallest vibration period of interest to ensure stability of the Newmark-Beta time integration (i.e. $\Delta t/T \leqslant 0.55$; e.g., Clough and Penzien [16]). The acceleration record is applied in these time steps to the SDoF system and the Newmark-beta time-integration method for linear acceleration is used to solve the dynamic nonlinear equilibrium equation for the evaluation of the SDoF response. The successive loading cycles follow a plain hysteretic curve with parallel unloading and reloading paths whose slope is the original elastic behavior of the structure, which do not currently account for pinching or for degradation of unloading stiffness. More advanced models will be considered in the future. The maximum response from the entire record defines the spectral displacements and accelerations used to characterize the demand at the AP. It is noted that the inelastic dynamic analysis only needs to be carried out on an SDoF system under the applied accelerogram at each AP, increasing the rapidity of the assessment.

2.5. Determination of the PP and EDPs

In ADRS space the AP on the capacity curve and the inelastic demand calculated for the matching inelastic SDoF (with elastic period and ductility determined by the idealized capacity curve to the AP) lie on a diagonal that passes through the origin and the AP. Although not used in the analysis, this diagonal theoretically represents the effective period of an equivalent linear SDoF. The inelastic demand and capacity curve can be directly compared along this diagonal, as they have the same ductility. If these points match, then the PP is reached. Exact matching is difficult to achieve from the predefined APs, which are spaced at subjective intervals

along the capacity curve. Hence, it can be beneficial to draw a "response curve" by joining together the inelastic demand values of S_a and S_d calculated at each analysis point, as the PP can be efficiently determined from the intersection of the capacity curve with this demand curve (see Fig. 1d).

In order to determine the EDPs corresponding to each PP, the capacity curve coordinates at the PP are used to determine the corresponding load step of the nonlinear static analysis file, and relevant response parameters (e.g. MIDR) are read from this file. Damage thresholds of EDP can be determined from an appropriately selected damage scale for the structure being analyzed (as discussed in Section 3.2).

2.6. Construction of fragility curves

In order to generate fragility functions, the capacity spectrum assessment is repeated for each structural model subjected to ground motions of increasing intensity, either by scaling each earthquake record or adopting a range of earthquake records with increasing intensity. A statistical curve fitting method is then adopted to fit a fragility curve shape from the IM - EDP cloud generated. Within FRACAS either a Least Squares (LS) approach or a Generalized Linear Model (GLM) can be used for the curve fitting, and confidence bounds derived using a bootstrap analysis of the data points. The former approach (LS) is more commonly used in the fragility literature but the method assumptions may be violated by the data, as shown by Rossetto et al. [17].

FRACAS has been developed into a Matlab-based automated tool, which is freely available at https://www.ucl.ac.uk/epicentre/resources/software or from the authors. This automated tool is used to carry out the analyses presented in the following sections to show the features of the developed approach.

3. Comparison of FRACAS with NLTHA

NLTHA provides a benchmark against which to test the performance of simplified capacity spectrum approaches like FRACAS. Hence, in this section the differences in EDP estimates obtained using FRACAS and NLTHA are investigated over a wide range of IM values, for two case-study reinforced concrete (RC) moment resisting frames (MRF). The resulting differences in derived fragility curves are also assessed.

3.1. The structural models and accelerograms

Two four-story four-bay RC MRF are selected for use in the comparison of FRACAS with NLTHA. These structures, which share the same geometry, represent distinct vulnerability classes, as they are characterized by different material properties and reinforcement detailing. The first frame is designed to only sustain gravity loads following the Italian Royal Decree n. 2239 of 1939 [18] that regulated the design of RC buildings in Italy up to 1971, hereafter called the Pre-Code building; the second frame is designed according to the latest Italian seismic code (or NIBC08; [19]), fully consistent with Eurocode 8 (EC8; [20]), following the High Ductility Class (DCH) rules, hereafter called the Special-Code building. Interstory heights, span of each bay and cross-sections dimensions for each case-study building are reported in Fig. 3. The considered frames are regular (both in plan and in elevation). Details regarding the design of the buildings are available in De Luca et al. [21].

In the case of the Pre-Code building, concrete with characteristic compressive strength f_{ck} = 19 MPa and reinforcement of characteristic yield stress f_{yk} = 360 MPa are used. In the case of the Special-Code building the characteristic compressive strength of concrete and the characteristic yield stress of steel reinforcement

used are f_{ck} = 29 MPa and f_{yk} = 450 MPa, respectively. Both frames are modelled using the finite element platform SeismoStruct [22]. The effect of confinement is taken into account by implementing the confinement model proposed by Mander et al. [23]. An insufficient level of confinement is observed in all sections of the Pre-Code building: the confinement factor, k, is defined as the confined-unconfined concrete compressive stress ratio and ranges from 1.01 to 1.05. The uniaxial hysteretic stress-strain relation proposed by Menegotto and Pinto [24] is used to represent the reinforcement steel behavior with the parameters proposed by Filippou et al. [25] for the inclusion of isotropic strain-hardening effects. To account for material inelasticity, a distributed plasticity approach is used. Thus each RC section consists of a total of 150 steel, confined concrete and unconfined concrete fibers.

Two sets of static PO analyses are carried out with different applied lateral load distributions, namely uniform and triangular. Lateral loads are incrementally applied to the side nodes of the structure. These lateral loads are proportionally distributed with respect to the local masses at each floor level (uniform distribution) and the interstory heights (triangular distribution). In both cases, the PO analysis is carried out until a predefined target displacement is reached, corresponding to the expected collapse state. Although APO approaches are generally perceived to provide better estimates of structure response than conventional static PO, particularly when higher modes and structural softening are important (as shown in many previous studies, such as [26]), it is decided not to adopt APO in the current comparison study. Inclusion of APO in FRACAS is computationally very expensive when dealing with a large number of unscaled accelerograms (as in the current study), as an APO needs to be developed for each accelerogram used.

Table 1 summarizes the structural and dynamic properties associated with each of the case-study building models, namely mass of the system m, fundamental period T_1 as well as the modal mass participation at the first mode of vibration.

Fig. 4 shows the static PO for the case-study buildings for both uniform (UNI-PO) and triangular (TRI-PO) lateral load distributions. The curves are reported in terms of top center-of-mass displacement divided by the total height of the structure (i.e., the roof drift ratio, RDR) along the horizontal axis of the diagram, and base shear divided by the building's seismic weight along the vertical axis (i.e., base shear coefficient). These figures show the capability of the structural model to directly simulate the response up to collapse. No significant difference is observed in the two pushover responses of the Pre-Code building and this is consistent with the available literature (e.g., [27]); both predict a soft story failure of the structure at its ground floor. In the case of the Special-Code building, the UNI-PO results in a base-shear capacity that is 5.7% higher than its TRI-PO counterpart, with damage predicted to be better distributed along the structure's height (again consistently with the available literature on the topic). These pushover analyses are adopted in the FRACAS assessment and are also used in Section 3.3 to define the structural response parameter thresholds of the damage limit states used in the fragility assessment.

A set of 150 unscaled ground motion records from the SIMBAD database (Selected Input Motions for displacement-Based Assessment and Design; [28]), is used to compare FRACAS with NLTHA and to test some of the model assumptions in FRACAS. SIMBAD includes a total of 467 tri-axial accelerograms, consisting of two horizontal (X-Y) and one vertical (Z) components, generated by 130 worldwide seismic events (including main shocks and aftershocks). In particular, the database includes shallow crustal earthquakes with moment magnitudes (M_w) ranging from 5 to 7.3 and epicentral distances R ⩽ 35 km. A subset of 150 records is considered here to provide a statistically significant number of strong-
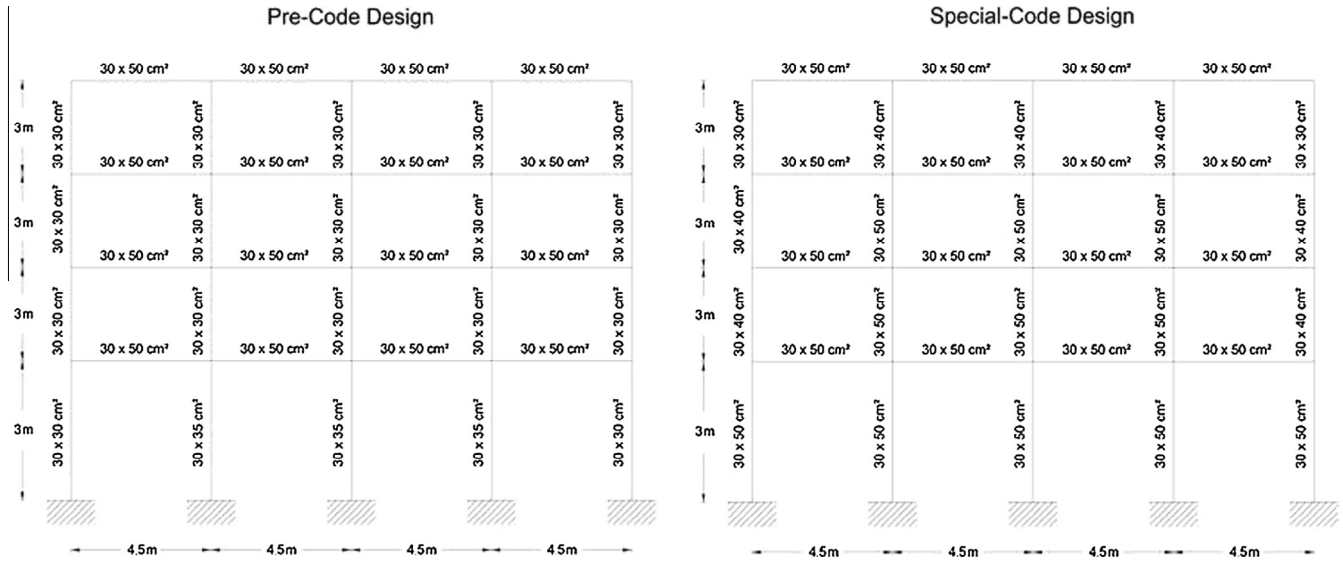
Fig. 3. Elevation dimensions and member cross-sections of the pre-code (left) and special-code (right) RC frames.

Table 1
Structural and dynamic properties of the case-study buildings.

Building type	Total mass, m [tonnes]	T_1 [s]	Modal mass participation (1st Mode) (%)
Pre-code	172.9	0.902	95.4
Special-code	172.9	0.506	92.8

motion records of engineering relevance for the applications presented in this paper. These records are selected by first ranking the 467 records in terms of their PGA values (by using the geometric mean of the two horizontal components) and then keeping the component with the largest PGA value (for the 150 stations with highest mean PGA).

3.2. Construction of fragility curves

In the following comparison, and in the rest of the paper, fragility functions are derived from the analysis (FRACAS or NLTHA) results by adopting thresholds of MIDR to define three damage states. The structure response characteristics associated with each damage state description are summarized in Table 2 and are based on a re-interpretation of the Homogenized Reinforced Concrete (HRC) damage scale of Rossetto and Elnashai [29] and that in Dolšek and Fajfar [30]. This has been necessary as no MIDR thresh-

olds are defined in the HRC Damage scale for RC MRF designed to modern seismic codes. The MIDR thresholds associated with each damage state are then derived from observations of when one of the identified response characteristics first occurs in the building's PO analysis. In this way the damage state EDP definitions are tailored to each building (see Table 2 for the thresholds used here for the two model structures). It is also noted that the HRC defined "Partial Collapse" limit state corresponds to the Dolšek and Fajfar [30] "Near Collapse" limit state and the Silva et al. [27] "Complete" damage limit state. These damage state definitions are used to generate all the fragility functions presented in this paper and the fragility curve parameters for all the functions shown in this paper are presented in Table A.1 in Appendix A.

In this paper, fragility curves are fit to the analysis data using the GLM approach with a Probit link function (see [17]). As mentioned in Section 2.6 the GLM model is theoretically more valid than LS, which assumptions are violated by the data used for the fragility assessment [17]. It is highlighted here that the choice of statistical model fitting technique may significantly influence the shape of the resulting fragility function. As an example, Fig. 5 shows the fragility functions obtained using GLM and LS for the Special-Code building assessed for the 150 unscaled records with FRACAS. It can be observed that the GLM and LS approaches result in large discrepancy between the fragility curves derived for DS2, with the GLM approach showing a greater variability in the results.
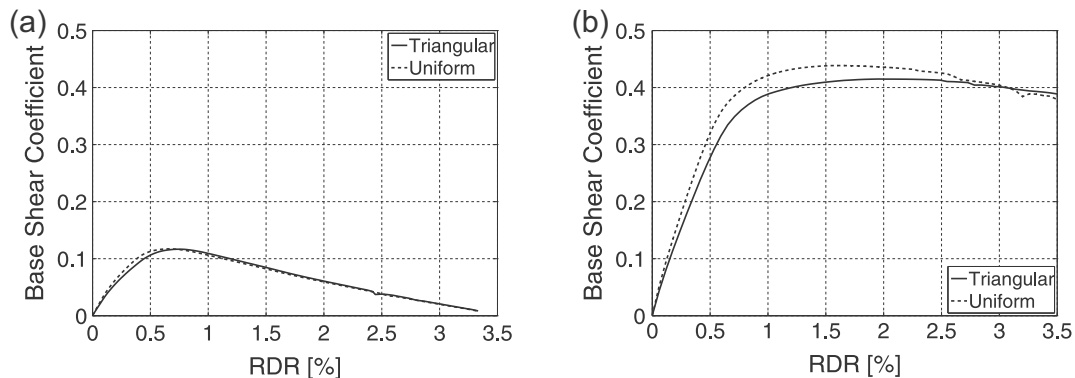

Fig. 4. Static PO curves for (a) the pre-code frame building and (b) the special-code building.

Table 2
Description of damage states and damage state thresholds used in this paper.

HRC damage state	DS$_1$ - Moderate	DS$_2$ - Extensive	DS$_3$ - Partial collapse
Observed damage	Cracking in most beams and columns. Some yielding in a limited number. Limited concrete spalling	Ultimate strength is reached in some elements	Failure of some columns or impending soft-story failure
Response characteristics (threshold defined by the first occurrence of any of these)	Global yield displacement, as obtained by the idealized curve[a]	Maximum moment capacity of a supporting column is reached	• There is a drop in strength to 80% of the maximum global capacity. • Shear failure of one element. • The rotation capacity of a critical column is reached.
MIDR threshold pre-code structure [%]	0.49	1.53	3.00
MIDR threshold special-code structure [%]	0.95	2.11	5.62

[a] In the present study, the EPP idealization model is used and the yielding point is determined using the first deviation (with an absolute gradient tolerance equal to 0.25).
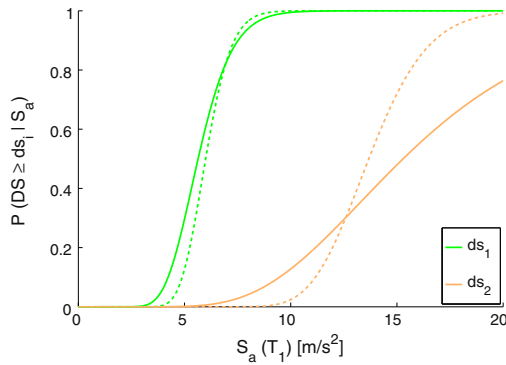

Fig. 5. Fragility functions derived by FRACAS using the GLM (sold lines) and the LS fitting (dashed lines) for the Special-Code building, TRI-PO, and EPP model.

The GLM better captures the fact that there are only a limited number of data points (observations) available for the higher damage states. It is noted, that despite the intensity of the chosen records being significant, too few data are available to derive the collapse damage state curve for the Special-Code building (without scaling the records). Hence, this damage state curve is not presented in the comparisons made in Section 3.3.

3.3. Comparison of FRACAS with NLTHA in terms of EDP estimates and fragility functions

Fig. 6 compares the MIDR values obtained from the NLTHA for the two frames with those estimated by FRACAS using the two pushover analyses as input. Results show that for both case-study structures FRACAS provides a reasonable estimate of the MIDR values predicted by NLTHA across the 150 ground motion records (average error is less around 25% across the considered models), particularly when nonlinear structural response is considered (average error is around 15% across the considered models). More in general, FRACAS generally tends to under-predict the MIDR values across the various IM levels and this is expected given the non-inclusion in the simplified method of (1) effect of higher modes (even in the elastic range of response) and (2) hysteresis models incorporating cyclic strength and stiffness deterioration. A non-negligible bias is observed for lower EDP due to the idealization of the capacity curve. In fact, the elastic branch of the idealized capacity model is obtained by directly connecting the origin to the first yield point, thus resulting in an initial stiffness (i.e., fundamental period) that is different from the one found for the actual structure. Therefore the structural response in the elastic range may also be strongly influenced by the chose idealization strategy.

There are indications in the capacity spectrum assessment literature that the choice of capacity curve idealization affects the resulting PPs (e.g. [9]). This is also observed by the authors. However, as discussed previously, one of the features of FRACAS is the ability to adopt different models for the capacity curve idealization. For instance, both TL and EPP idealizations were trialed to represent the response of the Pre-Code structure, which displays a (monotonic) degrading response curve after its maximum capacity. It is observed that the TL idealization results in a better approximation of the MIDR predicted by NLTHA than the EPP idealization, particularly near collapse. Furthermore, in carrying out this assessment a high sensitivity to the selected shape of the TL curve was observed. Despite this, the choice of capacity curve idealization does not significantly affect the resulting FRACAS fragility curves, as seen in Fig. 7, particularly when the GLM approach is employed in the statistical fitting. A greater effect may be observed for struc-
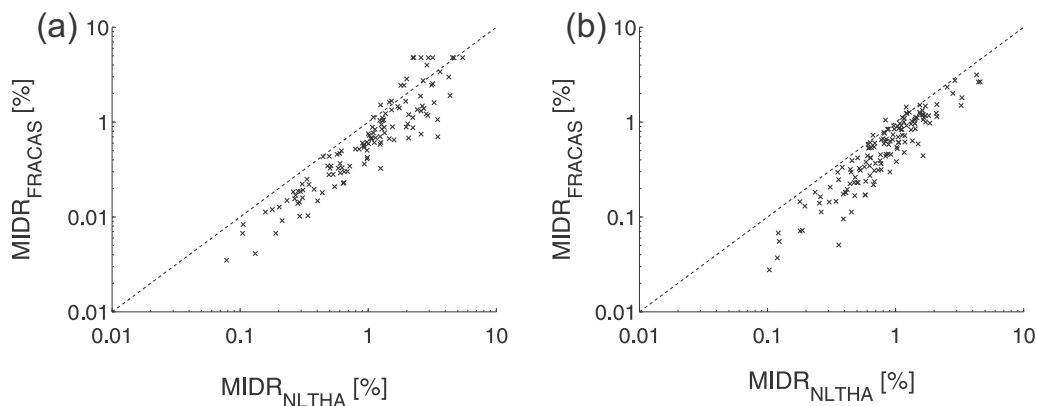

Fig. 6. Comparison of FRACAS with NLTHA in terms of MIDR: (a) pre-code building, TRI-PO, and TL and (b) special-code building, TRI-PO, and EPP model.
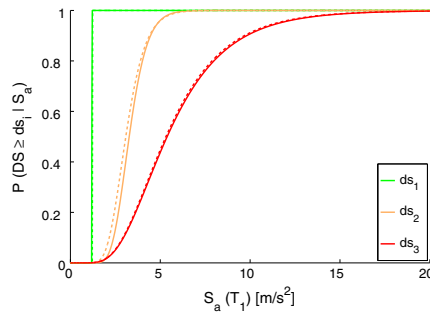
Fig. 7. Fragility functions derived by FRACAS using TL (solid lines) and EPP (dashed lines) for pre-code building and TRI-PO.

tures with infill where the PO curve presents different successive phases due to the failure of infill panels and where the EPP idealization provides a very poor fit to the PO curve. This will be investigated in future studies.

Comparisons between fragility functions developed using NLTHA as compared to simplified assessment methods is not often presented in the literature, and so it is discussed here. As expected, the under-prediction in EDPs by FRACAS is seen to translate directly into a lower fragility prediction compared to NLTHA (see Fig. 8). Despite this, it is observed that the two assessment methods provide similar fragility functions for all damage states of the Pre-Code building. However, larger discrepancies are observed for the Special-Code building, especially for the D2 damage state. These discrepancies are actually observed to arise from the sensitivity of the fragility curve fitting (in both approaches) to small numbers of observations rather than from the ability of FRACAS to simulate the NLTHA response of the building. For example, only 8 out of 150 records result in damage DS2 in the Special-Code building when NLTHA is employed, compared to only 5 in the case of FRACAS. These number further decrease when looking at damage DS3. The development of general guidelines as to how many analyses are required to create stable fragility functions, particularly when cloud-type approaches are used, is a subject of active research by several authors (e.g. [31]) and not investigated here, however the importance of considering this is highlighted by this example. Overall, FRACAS is observed to predict well the EDP response observed in NLTHA to failure in the case of the Pre-Code building, and hence only this structure is adopted in the following sections of the paper where a study of the ability of FRACAS to capture the effect of record-to-record variability on fragility functions is presented.
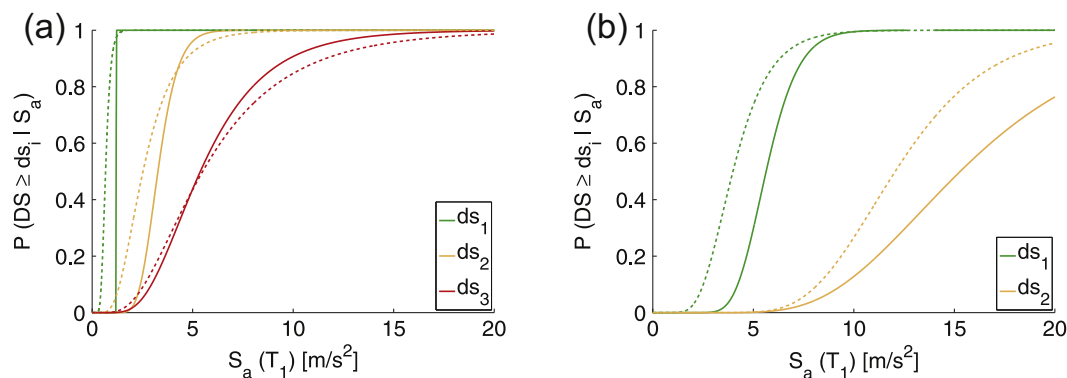
4. Investigation of the effect of record-to-record variability on fragility curves

To investigate the effect of record-to-record variability on fragility curves, the Pre-Code building presented in Section 3.1 is assessed under different suites of appropriately selected accelerograms using FRACAS. As the aim is to show how FRACAS captures the response spectral variability and translates it into fragility curves, natural accelerograms (i.e., recorded during past earthquake events) are selected and modified records are generated, based on the match of their spectra to a target spectrum. Although the current best practice does not require the compatibility or the matching with a given target spectrum (contrary to code-based procedures for single structures; e.g. [32]) neither does it recommend the use of a single hazard level (i.e., corresponding to just one return period of the seismic hazard) for fragility analysis (e.g., [33]), the approach followed here is deemed appropriate to investigate whether FRACAS is able to capture record-to-record variability.

4.1. Earthquake spectrum and input accelerograms for the structural assessment

The base spectrum chosen to carry out the structural assessment in FRACAS is the Type 1 EC8 [20] spectrum for soil class B (stiff soil), with a PGA of 0.17 g for a 475-year return period (i.e., 10% probability of exceedance in 50 years). This PGA is taken directly from the detailed probabilistic seismic hazard assessment (PSHA) of Stucchi et al. [34] for Italy and corresponds to a site located in Naples, Southern Italy, representative of moderate-to-high seismicity regions. Sets of accelerograms are chosen such that their mean spectrum matches the base spectrum over structural response periods 0.05–2 s with a lower limit tolerance of 10%. As EC8 does not provide any restrictions on the higher limit tolerance of the selected records, a maximum higher limit tolerance of 30% is arbitrarily selected (e.g., [35]). EC8 Section 3.2.3.1.2 does instead provide guidance on the relevant range of structural periods over which to carry out the matching, specifying this range in terms of the structural fundamental period of vibration (T_1) as $0.2T_1$ to $2T_1$. In the case of the considered case-study structure (Pre-Code building), the latter period range lies well within the adopted period range for matching. In the case of the natural records, the software REXEL [35] is used to select unscaled accelerograms from the three databases included in the software, namely Selected Input Motions for displacement-Based Assessment and Design (SIMBAD, [28]), the European Strong-motion Database (ESD) [36] and the Italian Accelerometric Archive (ITACA) [37]. It is worth noting that

Fig. 8. Fragility functions derived by FRACAS (solid line) and NLTHA (dashed line): (a) Pre-code building, TRI-PO, and TL and (b) special-code building, TRI-PO, and EPP model.

Table 3
Summary of record data returned by REXEL for the REAL-EC8:475 set.

| ID	Earthquake name	Date	M_w	Fault mechanism	Epicentral distance [km]	EC8 Site class	Database
147y	Friuli (aftershock)	9/15/1976	6	thrust	14	B	ESD
198x,y	Montenegro	4/15/1979	6.9	thrust	21	A	ESD
333x,y	Alkion	2/24/1981	6.6	normal	20	C	ESD
879y	Dinar	10/1/1995	6.4	normal	8	C	ESD
1726y	Adana	6/27/1998	6.3	strike slip	30	C	ESD
103y	Friuli (aftershock)	9/15/1976	5.9	thrust	16	A	ITACA
171y	Irpinia	11/23/1980	6.9	Normal	19	B	ITACA
381x	Umbria-Marche (aftershock)	9/26/1997	6	Normal	6	D	ITACA
22x	W Tottori Prefecture	10/6/2000	6.6	strike-slip	19	B	SIMBAD
146x	S Suruga Bay	8/10/2009	6.2	reverse	25	B	SIMBAD
411y	Hyogo - Ken Nanbu	1/16/1995	6.9	strike-slip	17	C	SIMBAD
437x	Parkfield	9/28/2004	6	strike-slip	10	B	SIMBAD
438x,y	Parkfield	9/29/2004	6	strike-slip	15	B	SIMBAD
443x	Imperial Valley	10/15/1979	6.5	strike-slip	25	B	SIMBAD
449x	Superstition Hills	11/24/1987	6.6	strike-slip	20	C	SIMBAD
458y	Northridge	1/17/1994	6.7	reverse	11	C	SIMBAD
459y	Northridge	1/18/1994	6.7	reverse	20	C	SIMBAD
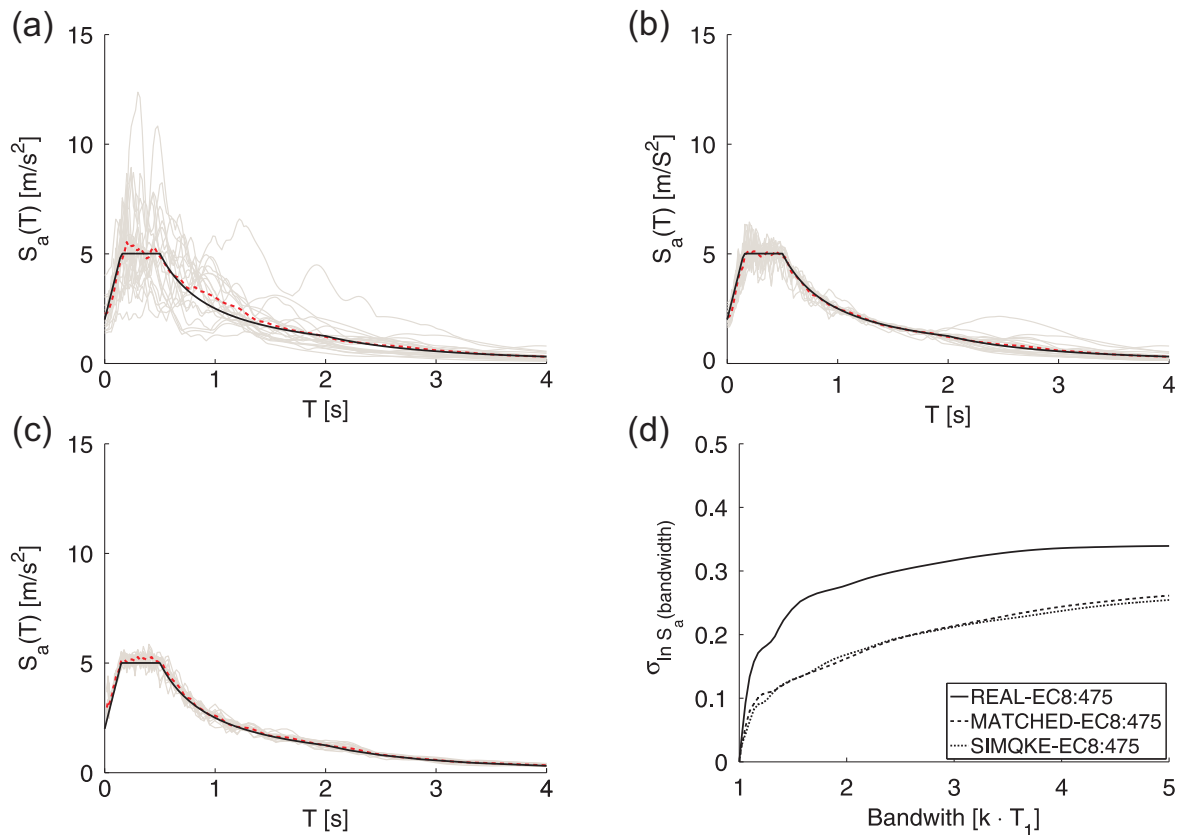
Fig. 9. (a)–(c) Elastic response spectra of the three sets of accelerograms (in grey), corresponding average (in red) and target spectrum used for the selection (in black): (a) REAL-EC8:475, (b) MATCHED-EC8:475, (c) SIMQKE-EC8:475; and (d) peak-to-trough variability of accelerograms. (For interpretation of the references to colour in this figure legend, the reader is referred to the web version of this article.)

the EC8 approach for ground motion selection is not sufficiently conservative for the derivation of fragility functions and this guideline has not been developed for this purpose. However, as discussed above, the main aim of the simple exercise carried out in this section is to demonstrate FRACAS' ability to capture record-to-record variability.

In particular, three suites of input accelerograms are adopted to assess the effect of record-to-record variability on the fragility curve produced for the Pre-Code building:

1. Twenty natural accelerograms (unscaled) to be compatible with the target spectrum over the period range 0.05–2 s (thereafter referred to as **REAL-EC8:475**).
2. The same accelerograms as in REAL-EC8:475 adjusted using wavelets so that their spectra better match the target (**MATCHED-EC8:475**). The program SeismoMatch [38] was adopted to adjust earthquake accelerograms to match a specific target response spectrum, using the wavelets algorithm proposed by Hancock et al. [39].
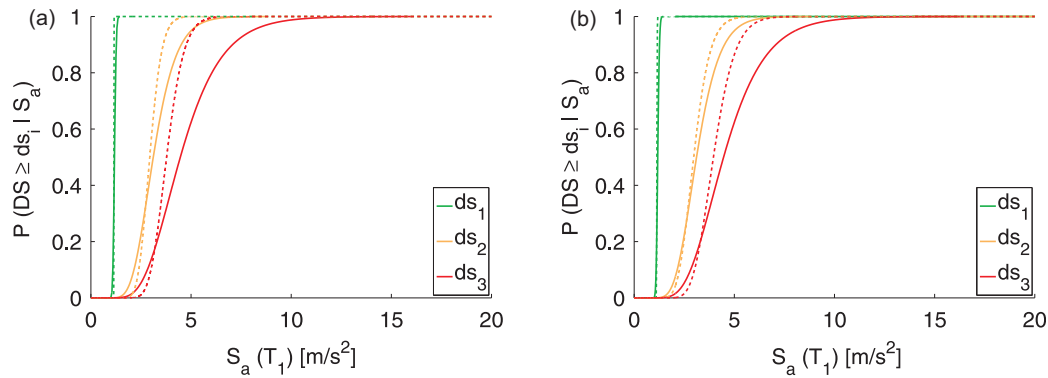
Fig. 10. Fragility functions by FRACAS using the three sets of accelerograms for the Pre-Code building, TRI-PO, and TL: (a) REAL-EC8:475 (solid lines) versus SIMQKE-EC8:475 (dashed lines) and (b) REAL-EC8:475 (solid lines) versus MATCHED-EC8:475 (dashed lines).
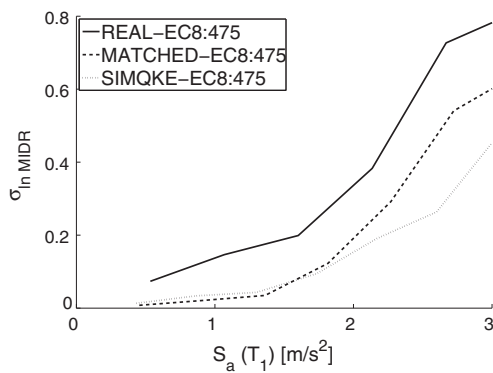

Fig. 11. Standard deviation of ln MIDR as a function of spectral acceleration for the pre-code building, TRI-PO, and TL.

3. Twenty accelerograms generated using SIMQKE [40], a method (and associated software) that can generate response-spectrum-compatible statistically-independent synthetic motions showing very little dispersion in their spectra and matching the target closely (**SIMQKE-EC8:475**).

Table 3 presents basic information on the ground motions used within the first two record sets. Within FRACAS these sets of accelerograms are scaled several times for the capacity spectrum assessment at increasing IM levels.

The elastic spectra for the three suites of accelerograms are shown in Fig. 9a–c together with their average, and the target spectrum. Stafford and Bommer [41] postulate that, when deriving fragility curves accounting for ground motion variability, the peak-to-trough variability in their response spectra should not be too small. They define the peak-to-trough variability as the standard deviation of the natural logarithm of spectral ordinates over a number of records and a range of response periods defined by the 'bandwidth', i.e. the range of periods surrounding a central period. This bandwidth roughly corresponds to the degree of structural nonlinearity that is expected and the contribution of higher mode effects. With the capacity spectrum method used here the structure is not affected by spectral ordinates with periods shorter than the natural period (equal to 0.902 s for the Pre-Code structure). Therefore, we modify the definition of the peak-to-trough variability to account for only those periods longer than the natural period. The peak-to-trough variability for each suite of accelerograms is plotted in Fig. 9d as function of an elongated period (equal to $k \cdot T_1$) rather than bandwidth.

Fig. 9 shows that, as expected, the MATCHED and SIMQKE records show similar but considerably less spectral variability than the natural accelerograms. The variability shows a similar behavior to that shown by Stafford and Bommer [41] but with higher absolute values.

4.2. Fragility assessment

For the construction of fragility functions the three suites of accelerograms presented in Section 4.1 are used to define the demand spectra and are combined with the capacity curves obtained from the PO analysis of the structure. FRACAS analyses are carried out on the Pre-Code building with each of the ground motion sets, scaled to varying spectral accelerations (S_a). Fragility curves are derived for each set of accelerograms (300 data points each, i.e. 20 original records scaled 15 times) using a GLM statistical curve fitting approach. The resulting curves follow a cumulative lognormal distribution with mean α and standard deviation β as the fragility parameters (i.e., the parameters of the associated normal distribution). The fragility curve parameters for all the functions are presented in Table A.1 in Appendix A.

Fig. 10 shows that the fragility curves derived for MATCHED-EC8:475 and SIMQKE-EC8:475 differ in both median and standard deviation from the fragility curves derived for the REAL-EC8:475 set, especially at the higher damage states. The initial record-to-record variability is efficiently translated to the final fragility curves, as shown by the different values of the standard deviation β. The use of scaled accelerograms allows the computation of the standard deviation of the MIDR within each bin of IM (i.e. set of 20 ground motions scaled according to $S_a(T_1)$), as shown in Fig. 11. It is noted that the variability in the structural response increases with the imposed intensity level: this observation emphasizes the role of the specific nonlinear computations that are performed in FRACAS during the estimation of the inelastic response spectrum. Once the yield limit is reached, the relation between the IM and the structural response shows high heteroscedasticity. The relative variability between the three sets of accelerograms also follows a similar trend to the peak-to-trough variability. It is highlighted that the dispersion in the structural response tends to stabilize or even decrease for higher intensities due to a peculiarity of FRACAS, which considers PPs exceeding the ultimate point as "collapse" events, and thus sets their value to the last point of the curve.

The reason for the different medians (α) of the MATCHED-EC8:475 and SIMQKE-EC8:475, compared to the REAL-EC8:475 fragility curves, particularly for DS3, could be related to the bias introduced by spectral matching recently evidenced by Seifried and Baker [42]. These authors studied the reason for the observed un-conservative bias in fragility curves when closely matched spectra are used (i.e. the effect that is observed when comparing

Table A.1
Fragility parameters (mean α in m/s^2 and standard deviation β).

Building	Capacity model	Ground motions	Derivation method	D1		D2		D3	
				α	β	α	β	α	β
Special code	NLTHA	Unscaled	GLM	3.987	0.360	12.059	0.300	–	–
	EPP	Unscaled	GLM	5.639	0.225	15.291	0.374	–	–
	EPP	Unscaled	LS	5.995	0.159	13.677	0.159	–	–
Pre-code	NLTHA	Unscaled	GLM	0.669	0.302	2.531	0.480	5.498	0.584
	TL	Unscaled	GLM	1.199	0.003	3.273	0.241	5.384	0.468
	EPP	Unscaled	GLM	1.230	0.002	3.084	0.277	5.317	0.467
	TL	REAL-EC8:475	GLM	1.179	0.056	3.115	0.289	4.466	0.359
	TL	SIMQKE-EC8:475	GLM	1.143	0.001	2.938	0.161	3.780	0.181
	TL	MATCHED-EC8:475	GLM	1.136	0.012	2.973	0.214	3.957	0.213

REAL-EC8:475 and MATCHED-EC8:475). They show that this bias is solely due to the loss of extreme spectral ordinates (i.e. peaks) in closely matched spectra, which are usually responsible for large deformations in the structural system: the nonlinear relation between the IM and EDP value (i.e. with higher IMs leading to a much larger EDPs variation than proportionally smaller IMs) coupled with the spectrum variability, therefore, explains the loss of higher EDP values when using closely matched spectra. This observation raises the question as to whether the natural record-to-record variability, which is originally not present for matched records, should be added back in during the final steps.

5. Conclusions

This paper presents a new approach for the derivation of fragility curves, named FRAgility through Capacity spectrum ASsessment (FRACAS). FRACAS adapts the capacity spectrum assessment method and uses inelastic response spectra derived from earthquake accelerograms to construct fragility curves. The paper compares the predicted MIDR response obtained by FRACAS and NLTHA for two case-study 4-story RC frames assessed under 150 accelerograms. FRACAS is seen to represent well the response of both case study structures when compared to NLTHA. The case study application also highlights the sensitivity of the FRACAS EDP predictions to the adopted capacity curve idealization, but shows an insensitivity of the derived fragility function to the idealization model choice so long as the idealization model provides a reasonable fit to the real capacity curve. The statistical model used to fit the fragility function is seen to have a significant influence on the resulting curves, and it is highlighted that the sensitivity of the fragility function to number of analyses must always be checked.

The paper also shows how FRACAS is able to capture the inelastic record-to-record variability and properly translate it into the resulting fragility curves. In particular, through an example application, it is shown that the variability in spectral ordinates for periods beyond the natural period of the undamaged structure is directly correlated to the standard deviations of the fragility curves. A variant of the peak-to-trough measure of the variability in the input spectra (accounting only for periods longer than the natural period) is proposed and is seen to provide a useful measure of this variability. Consequently, it is concluded that differences between fragility curves derived using static PO approaches can be partially explained by differences in the input spectra, even if the mean target spectra are similar.

Overall, the paper demonstrates that FRACAS is able to represent the effects of record-to-record variability in fragility curves, and has the advantage of simplicity and rapidity over other methods that use accelerograms directly.

Appendix A. Parameters for all derived fragility curves

Table A.1.

References

[1] D'Ayala D, Meslem A, Vamvatsikos D, Porter K, Rossetto T, Crowley H, Silva V. Guidelines for analytical vulnerability assessment, vulnerability global component project. Pavia: GEM foundation; 2014.

[2] Vamvatsikos D, Cornell CA. Incremental dynamic analysis. Earthquake Eng Struct Dynam 2002;31(3):491–514. http://dx.doi.org/10.1002/eqe.141.

[3] Jalayer F, Cornell CA. Alternative nonlinear demand estimation methods for probability-based seismic assessments. Earthquake Eng Struct Dynam 2009;38(8):951–72.

[4] Freeman SA, Nicoletti JP, Tyrell JV. Evaluations of existing buildings for seismic risk – a case study of puget sound naval shipyard, Bremerton, Washington. In: Proceedings of U.S. national conference on earthquake engineering. Berkeley. p. 113–22.

[5] ATC. Seismic evaluation and retrofit of concrete building. Report (ATC-40). California: Applied Technology Council; 1996.

[6] FEMA. FEMA 356: prestandard and commentary for the seismic rehabilitation of buildings. Publication n°356. The American Society of Civil Engineers for the Federal Emergency Management Agency: Washington; 2000.

[7] Fajfar P. Capacity spectrum method based on inelastic demand spectra. Earthquake Eng Struct Dynam 1999;28:979–93.

[8] Fajfar P. A nonlinear analysis method for performance-based seismic design. Earthquake Spectra 2000;16(3):573–92.

[9] Rossetto T, Elnashai A. A new analytical procedure for the derivation of displacement-based vulnerability curves for populations of RC structures. Eng Struct 2005;27:397–409.

[10] Gehl P, Douglas J, Rossetto T, Macabuag J, Nassirpour A, Minas S, Duffour P. Investigating the use of record-to-record variability in static capacity spectrum approaches. In: Proceedings of ASCE-ICVRAM-ISUMA conference. Liverpool.

[11] Rossetto T, Gehl P, Minas S, Nassirpour S, Macabuag J, Duffour P, Douglas J. Sensitivity analysis of different capacity approaches to assumptions in the modeling, capacity and demand representations. In: Proceedings of ASCE-ICVRAM-ISUMA conference. Liverpool.

[12] Silva V, Crowley H, Pinho R, Varum H. Investigation of the characteristics of Portuguese regular moment-frame RC buildings and development of a vulnerability model. Bull Earthq Eng 2014;13(5):1455–90.

[13] Elnashai AS. Advanced inelastic static (pushover) analysis for earthquake applications. Struct Eng Mech 2001;12(1):51–69.

[14] Rossetto T. Vulnerability curves for the seismic assessment of reinforced concrete building populations Ph.D. Thesis. London: Department of Civil and Environmental Engineering, Imperial College; 2004.

[15] De Luca F, Vamvatsikos D, Iervolino I. Near-optimal piecewise linear fits of static pushover capacity curves for equivalent SDOF analysis. Earthquake Eng Struct Dynam 2013;42(2):523–43. http://dx.doi.org/10.1002/eqe.2225.

[16] Clough R, Penzien J. Dynamics of structures. New York: McGraw Hill Inc; 1993.

[17] Rossetto T, Ioannou I, Grant D, Maqsood T. Guidelines for empirical vulnerability assessment. GEM Technical Report. Pavia: GEM Foundation; 2014. http://dx.doi.org/10.13140/2.1.1173.4407.

[18] Reggio Decreto 16/11/1939 n. 2229. Norme per la esecuzione delle opere in conglomerato cementizio semplice e armato. G.U. n. 92 del 18/04/1940 [in Italian].

[19] Italian Building Code. Norme Tecniche per le Costruzioni. Rome: Gazzetta Ufficiale della Repubblica Italiana; 2008 [in Italian].

[20] EN 1998-1. Eurocode 8: Design of structures for earthquake resistance – part 1: general rules, seismic actions and rules for buildings. [Authority: The European Union Per Regulation 305/2011, Directive 98/34/EC, Directive 2004/18/EC]: Brussels; 2004.

[21] De Luca F, Elefante L, Iervolino I, Verderame GM. Strutture esistenti e di nuova progettazione : comportamento sismico a confronto. In: Anidis 2009 XIII Convegno – L' ingegneria Sismica in Italia. Bologna; 2009 [in Italian].

[22] SeismoSoft. SeismoStruct: a computer program for static and dynamic nonlinear analyzes of framed structures Available at:Available from: <http://www.seismosoft.com>2007.

[23] Mander JB, Priestley MJN, Park R. Theoretical stress-strain model for confined concrete. ASCE J Struct Eng 1988;114(8):1804–26.

[24] Menegotto M, Pinto PE. Method of analysis for cyclically loaded RC plane frames including changes in geometry and non-elastic behaviour of elements under combined normal force and bending. In: Proceedings of symposium on the resistance and ultimate deformability of structures anted on by well defined loads. Lisbon.

[25] Filippou FC, Popov EP, Bertero VV. Effects of bond deterioration on hysteretic behavior of reinforced concrete joints. Report EERC 83-19. Berkeley: Earthquake Engineering Research Center, University of California; 1983.

[26] Antoniou S, Pinho R. Development and verification of a displacement-based adaptive pushover procedure. J Earthquake Eng 2004;8:643–61.

[27] Silva V, Crowley H, Varum H, Pinho R, Sousa R. Evaluation of analytical methodologies used to derive vulnerability functions. Earthquake Eng Struct Dynam 2014;43:181–204.

[28] Smerzini C, Galasso C, Iervolino I, Paolucci R. Ground motion record selection based on broadband spectral compatibility. Earthquake Spectra 2014;30(4):1427–48. http://dx.doi.org/10.1193/052312EQS197M.

[29] Rossetto T, Elnashai AS. Derivation of vulnerability functions for European-type RC structures based on observational data. Eng Struct 2003;25(10):1241–63.

[30] Dolšek M, Fajfar P. The effect of masonry infills on the seismic response of a four-storey reinforced concrete frame – a deterministic assessment. Eng Struct 2008;30(7):1991–2001.

[31] Gehl P, Douglas J, Seyedi D. Influuence of the number of dynamic analyse on the accuracy of structural response estimates. Earthquake Spectra 2015;31(1):97–113.

[32] NIST. Selecting and scaling earthquake ground motions for performing response-history analyses. NIST GCR 11-917-15. Prepared by the NEHRP Consultants Joint Venture for the National Institute of Standards and Technology: Gaithersburg (MD); 2011.

[33] Lin T, Baker JW. Introducing adaptive incremental dynamic analysis: a new tool for linking ground motion selection and structural response assessment. In: 11th International conference on structural safety and reliability. New York.

[34] Stucchi M, Meletti C, Montaldo V, Crowley H, Calvi GM, Boschi E. Seismic hazard as-sessment (2003–2009) for the Italian building code 2011. Bull Seismol Soc Am 2011;101:1885–911.

[35] Iervolino I, Galasso C, Cosenza E. REXEL: computer aided record selection for code-based seismic structural analysis. Bull Earthq Eng 2009;8:339–62. http://dx.doi.org/10.1007/s10518-009-9146-1.

[36] Ambraseys N, Smit P, Douglas J, Margaris B, Sigbjörnsson R, Olafsson S, Suhadolc P, Costa G. Internet site for European strong-motion data. Bollettino di Geofisica Teorica ed Applicata 2004;45(3):113–29.

[37] Pacor F, Paolucci R, Luzi L, Sabetta F, Spinelli A, Gorini A, Nicoletti M, Marcucci S, Filippi L, Dolce M. Overview of the Italian strong motion database ITACA 1.0. Bulletin. Earthq Eng 2011;9(6):1723–39. http://dx.doi.org/10.1007/s10518-011-9327-6.

[38] SeismoSoft. SeismoMatch v2.1 – a computer program for spectrum matching of earthquake records Available at:Available from: <http://www.seismosoft.com>2007.

[39] Hancock J, Watson-Lamprey J, Abrahamson N, Bommer J, Markatis A, McCoy E, Mendis R. An improved method of matching response spectra of recorded earthquake ground motion using wavelets. J Earthq Eng 2006;10(1):67–89.

[40] Gasparini DA, Vanmarcke EH. SIMQKE: a program for artificial motion generation. Cambridge: Department of Civil Engineering, Massachusetts Institute of Technology; 1976.

[41] Stafford PJ, Bommer JJ. Theoretical consistency of common record selection strategies in performance-based earthquake engineering. Advances in performance-based earthquake engineering. Geotech, Geol Earthq Eng 2010;13:49–58.

[42] Seifried AE, Baker JW. Spectral variability and its relationship to structural response estimated from scaled and spectrum-matched ground motions. In: 10th U.S. national conference on earthquake engineering, frontiers of earthquake engineering. Anchorage (Alaska).